Acta Neuropathologica (2022) 144:691–706
https://doi.org/10.1007/s00401-022-02463-y

ORIGINAL PAPER

Flow blockage disrupts cilia-driven fluid transport in the epileptic brain

Regina J. Faubel[1] · Veronica S. Santos Canellas[1] · Jenna Gaesser[2] · Nancy H. Beluk[3] · Tim N. Feinstein[1] · Yong Wang[4] · Maya Yankova[5] · Kalyani B. Karunakaran[6] · Stephen M. King[5] · Madhavi K. Ganapathiraju[7] · Cecilia W. Lo[1]

Received: 4 April 2022 / Revised: 27 June 2022 / Accepted: 28 June 2022 / Published online: 18 August 2022

Abstract

A carpet of ependymal motile cilia lines the brain ventricular system, forming a network of flow channels and barriers that pattern cerebrospinal fluid (CSF) flow at the surface. This CSF transport system is evolutionary conserved, but its physiological function remains unknown. Here we investigated its potential role in epilepsy with studies focused on CDKL5 deficiency disorder (CDD), a neurodevelopmental disorder with early-onset epilepsy refractory to seizure medications and the most common cause of infant epilepsy. *CDKL5* is a highly conserved X-linked gene suggesting its function in regulating cilia length and motion in the green alga *Chlamydomonas* might have implication in the etiology of CDD. Examination of the structure and function of airway motile cilia revealed both the CDD patients and the *Cdkl5* knockout mice exhibit cilia lengthening and abnormal cilia motion. Similar defects were observed for brain ventricular cilia in the *Cdkl5* knockout mice. Mapping ependymal cilia generated flow in the ventral third ventricle (v3V), a brain region with important physiological functions showed altered patterning of flow. Tracing of cilia-mediated inflow into v3V with fluorescent dye revealed the appearance of a flow barrier at the inlet of v3V in *Cdkl5* knockout mice. Analysis of mice with a mutation in another epilepsy-associated kinase, Yes1, showed the same disturbance of cilia motion and flow patterning. The flow barrier was also observed in the $Foxj1^{\pm}$ and $FOXJ1Cre^{ERT}{:}Cdkl5^{y/fl}$ mice, confirming the contribution of ventricular cilia to the flow disturbances. Importantly, mice exhibiting altered cilia-driven flow also showed increased susceptibility to anesthesia-induced seizure-like activity. The cilia-driven flow disturbance arises from altered cilia beating orientation with the disrupted polarity of the cilia anchoring rootlet meshwork. Together these findings indicate motile cilia disturbances have an essential role in CDD-associated seizures and beyond, suggesting cilia regulating kinases may be a therapeutic target for medication-resistant epilepsy.

Keywords Cerebrospinal fluid · Seizure · Cilia · Epilepsy · Transport · Homeostasis

✉ Cecilia W. Lo
cel36@pitt.edu

[1] Department of Developmental Biology, University of Pittsburgh School of Medicine, Pittsburgh, PA 15201, USA

[2] Division of Child Neurology, Department of Pediatrics, University of Pittsburgh School of Medicine, Pittsburgh, PA 15201, USA

[3] Division of Radiology, University of Pittsburgh, Pittsburgh, PA 15260, USA

[4] Laboratory for Fluid Physics, Pattern Formation and Biocomplexity, Max Planck Institute for Dynamics and Self-Organization, Am Faßberg 17, 37077 Göttingen, Germany

[5] Department of Molecular Biology and Biophysics, And Electron Microscopy Facility, University of Connecticut Health Center, Farmington, CT 06030-3305, USA

[6] Supercomputer Education and Research Centre, Indian Institute of Science, Bangalore 560012, India

[7] Department of Biomedical Informatics, University of Pittsburgh School of Medicine, Pittsburgh, PA 15201, USA

Introduction

Epilepsy is a common neurologic disorder with a recurrent seizure that affects 1% of the population. A third of all epilepsies are non-responsive to treatment, suggesting the current focus on synaptic and voltage-gated conductances might be inadequate [31, 34, 42]. Pathogenic mechanisms in many epilepsies are poorly understood, but homeostatic imbalances in brain physiology are a universal aspect of seizure [42]. The discrepancy between actual mechanisms of seizure versus the focus of research is further demonstrated by the overrepresentation of metabolic functions among seizure-related genes and not of neuron-specific functions such as ion channels or neurotransmitter agonists and antagonists that are in the focus of mouse epilepsy models and currently available seizure medications (Fig. SI1).

Here, we investigated the possible role of cilia-driven fluid transport in the brain ventricles as a novel epileptogenic mechanism. This focus was suggested by the unexpected finding that CDKL5 (Cyclin-dependent kinase-like 5), an X-linked kinase that is highly conserved from the unicellular alga *Chlamydomonas* to man regulates motile cilia function. *Chlamydomonas cdkl5* mutants show lengthening and abnormal bending of the flagellum, a motile cilium mediating cell locomotion, and thus exhibit abnormal swimming behavior [43]. Significantly, this gene is also associated with a neurodevelopmental disorder referred to as CDKL5 deficiency disorder (CDD) [33]. CDD is one of the most common causes of medication-resistant seizures in the infant/pediatric population. Intractable seizures in CDD patients usually begin within a few weeks to months of birth [12]. CDD is associated with severe neurodevelopmental delay accompanied by intellectual disability and motor, speech and visual deficits, as well as the disturbance of other physiological functions such as sleep and gastrointestinal function [23, 33]. Some new insights into the pathogenic mechanisms for CDD have come from studies in *Cdkl5* knockout (KO) mouse models [1, 3, 14, 44, 46, 49], and in vitro studies of retinal pigmental epithelial cells and brain organoids generated from CDD patient induced pluripotent stem cells [7, 30]. However, the underlying pathogenic mechanisms for uncontrollable seizures in CDD remains poorly understood. Due to this lack of insights into mechanisms, it has not been possible to develop targeted therapies to treat the uncontrollable seizures in CDD.

Thus we investigated the impact of CDKL5 deficiency on motile cilia in CDD patients and *Cdkl5* knockout (KO) mice, and its potential contribution to seizure susceptibility. We focused these studies on ependymal cilia in the ventral third ventricle (v3V), a recessed cavity lined by neurosecretory nuclei of the hypothalamus that have important roles in regulating a wide spectrum of physiological functions such as appetite control, circadian rhythm, and emotion [10]. We previously documented the presence of an intricate ependymal cilia-driven fluid transport system in the v3V that is evolutionarily conserved among mammals [10]. Furthermore, we observed that cilia beating direction and flow pattern in the v3V changes predictable by the time of day and night [10]. In this current study, we investigated and obtained evidence that such cilia-driven fluid transport in the v3V is altered by motile cilia disturbances associated with CDD. An altered flow pattern was found to be closely associated with increased seizure susceptibility. We provide evidence that this requires Cdkl5 function in the multiciliated brain ependymal cells and arises from defects in cilia-generated flow caused by the disrupted polarity of a ciliary rootlet anchoring meshwork.

Materials and methods

Human subject recruitment and CDD patient clinical history

This study was conducted under a human study protocol approved by the University of Pittsburgh Institutional Review Board and, therefore, are in accordance with the 1964 Declaration of Helsinki. Control subjects and CDD patients (Table S1) were recruited with written informed consent by either adult subjects or the parents of the two patients with CDD. Female CDD patient P1 began having seizures at 5 weeks of age and was diagnosed with CDD after genetic testing at 11 months of age revealed a de novo splicing defect mutation absent from either parent. She has 3–6 tonic seizures per day that are intractable and refractory to treatment. CDD patient P2 began having seizures at 3 weeks of age, with genetic testing confirming a diagnosis of CDD at 13 months of age.

Imaging the respiratory cilia from human subjects and mice

Nasal samples were obtained from 5 control subjects and 2 CDD patients for analysis of respiratory motile cilia function. Samples were collected with a nasal scrape performed using a rhinoprobe and the tissue kept in L15 medium until imaging (Life Technologies, 21083-027). For the mouse airway, trachea was obtained after euthanasia, with strips of the tracheal epithelia dissected for videomicroscopy. The human nasal tissue collected was mounted on covered glass-bottom dishes (Glass bottom microwell dishes; MatTek P-35G-1.5-10-C) and imaged using differential interference contrast

(DIC) optics with a 100X oil objective under a Leica inverted microscope (DMI 3000) equipped with Phantom v4.2 camera (Vision Research). For mouse trachea, strips of the tracheal epithelia were secured luminal side down on the glass-bottomed dish and cilia dynamics were captured along the edge of the trachea strips using the same 100X oil objective with DIC optics with the Phantom camera. Videos were recorded using 200 frames per sec and later used for the analysis of airway cilia dynamics.

Mouse breeding and mouse lines

All mouse studies were conducted under an animal study protocol approved by the University of Pittsburgh Institutional Animal Care and Use Committee and the "Principles of laboratory animal care" (NIH publication No. 86-23, revised 1985) were followed in compliance with specific state laws of Pennsylvania, USA. The mice were maintained with 12:12 h light:darkness cycle and fed ad libitum with regular chow. The mouse lines used in this study included C57BL/6 J wildtype mice, *Cdkl5* KO [49], and *FoxJ1*$^{\pm}$ [29] mice obtained from the Jackson Laboratory and further bred in our mouse colony and maintained in the C57BL6/J background. Mice carrying floxed alleles of *Cdkl5* (*Cdkl5*$^{fl/fl}$ and *Cdkl5*$^{y/fl}$) were kindly provided by Dr. Zhaolan Zhou (University of Pennsylvania) [44]. The *FOXJ1Cre*^{ERT} mice were kindly provided by Dr. Chay Kuo (Duke University) [36]. Also included in this study is a *Yes1* mutant (*Yes1*$^{+/mt}$) mouse line harboring a missense mutation (c.T4304C:p.L1435P) generated by CRISPR gene editing. This mutation was first identified from a mouse mutagenesis screen and found to cause congenital heart defect with low penetrance [24].

Anesthesia induced seizure assay

A seizure assay was developed to assess seizure susceptibility in mice based on the previous report of seizures in patients during anesthesia with volatile anesthetics such as isoflurane [48, 53], and the findings in mice that isoflurane exposure induces the release of metabolites [18] which has the potential to trigger seizure if not cleared from the CSF. For this assay, mice were anesthetized by administration of 4% Isoflurane mixed with 2% oxygen, followed by placement into a transparent plexiglass anesthesia induction chamber allowing continuous visual assessment of the mice. The chamber is filled with 4% isoflurane with 2% oxygen for induction of anesthesia. After 30 s induction phase, mouse activity was video recorded over the next 35 s in 5 s intervals to track any involuntary motion or convulsions. Subsequently, isoflurane was stopped while oxygen levels were kept at 2% until the mice awaken. To assess the seizure activity score during each 5 s interval, a score of 1 is given for any motion and 0 for no motion, with the resulting score was used to calculate the percentage of mice exhibiting anesthesia-triggered involuntary motion. Second, the videos were further reviewed and scored using a modified racine scale, with 0 for each second with no motion, 1 for whisker trembling and nodding, 2 limb, tail or head twitching or, circular turning of the body by up to 180 degrees, 3 flipping to one side and mild clonic seizure. 4 the body turning a full circle, flipping on the back, clonic-myotonic seizure of the whole body or clonus standing on the hindlegs. For each mouse, the scores summed for 5 s intervals over the 35 s observation period provided the anesthesia-induced seizure score. For quantification of seizure scores, *t* test was performed. The seizures assay was conducted on 4 *FoxJ1*$^{\pm}$ mice and 4 littermate controls age 5–6 weeks, 9 *Cdkl5* KO mice and 7 *Yes1*$^{+/mt}$ mice aged 2–5 months and 7 age-matched wildtype control mice.

Confocal immunofluorescence microscopy

Immunostaining was conducted with cells obtained from the respiratory epithelia of human nasal scrapes or murine trachea, and the mouse brain ependyma from the v3V. Cells retrieved from these tissues were attached to polylysine-coated cover glass (Glass bottom microwell dishes; MatTek P-35G-1.5-10-C) at 37 °C for 2 h and subsequently fixed in 5% Paraformaldehyde (PFA) in 1 × TBS (Fisher BioReagents™, BP2471-1) for 15 min, blocked in 10% Bovine serum albumin (BSA) in TBS with 1% Triton X-100 (Sigma T9284) for one hour at room temperature, incubated in primary antibody solution overnight at 4 °C. Then samples were transferred to secondary antibody solution for one hour at room temperature and washed three times in TBS with 1% Triton X-100 (Sigma T9284). Cell was then mounted in Prolong™ Glass Antifade Mountant (Invitrogen) and imaged using a Leica SP8 confocal microscope with 63× magnification. The primary antibodies used included: rabbit anti-CROCC antibody (Novus, Nbp-80820), anti-acetylated tubulin monoclonal antibody (Sigma T7451), rabbit monoclonal antibody to PAK2 (abcam ab76293), monoclonal gamma-tubulin antibody (Sigma T6557). Secondary antibodies used included AlexaFluor™ 647 donkey anti-rabbit IgG (Invitrogen A31573), AlexaFluor™ 555 anti-mouse IgG2b (Invitrogen A21147), and AlexaFluor™ 488 anti-mouse IgG1 (Invitrogen A21121). Antibody solution included 1:1000 dilution in TBS with 1%Triton X-100 and 3% BSA. Orientation of rootletin-immunostained cellular structures was determined using Fiji [38]. Eccentricity for the pattern of rootletin-immunostaining was determined as the ratio of the short vs. long axis of the rootletin immunostained area in each cell. Analysis was conducted on 5 mice for each genotype, with a total number of cells analyzed for wild-type mice being $n = 433$, *Cdkl5* KO $n = 991$, *Yes1*$^{+/mt}$ $n = 612$.

Live ependymal tissue imaging

Mice were euthanized and the brain removed and placed in DMEM (Life Technologies 11960-044). Using razor blades, a coronal slice was obtained with a thickness of about 3 mm that comprise the hypothalamus. With electrolytically sharpened needles, the v3V was cut open and the walls of the v3V were further dissected and imaged in cilia-imaging chambers as previously described [10]. Bead propagation with the cilia-generated flow was recorded at 30 fps on a DMLFSA microscope (Leica) with an EM-CCD camera (Hamamatsu, C9100). Ciliary motion was imaged using DIC optics on a DMI3000 microscope (Leica) equipped with a Phantom camera. The flow maps generated for Fig. 3 were based on data collected from $n=10$ *Cdkl5* KO and $n=10$ age-matched C57BL6 wildtype mice at 2–4 months of age. For Figs. 4, 5 *Yes*$^{+/mt}$ mice were analyzed at 2–4 months of age. For flow maps in Fig. 5, $n=4$ *FoxJ1*$^{\pm}$ and $n=4$ age-matched *FoxJ1*$^{+/+}$ littermate controls at 5–6 weeks of age and $n=8$ for Cdkl5$^{y/fl}$ mice carrying the tamoxifen-inducible FOXJ1Cre^{ERT} at 4 weeks of age and 7 littermates, respectively, age-matched controls without FOXJ1Cre^{ERT}. Ependyma-specific KO was induced by maternal administration of Tamoxifen at postnatal days 1,3 and 5. Ependymal cilia length measurements were obtained with analysis conducted on $n=4$ wildtype mice, $n=4$ *Cdkl5 KO* mice, $n=3$ *Yes1*$^{+/mt}$ mice (Online Resource 1).

Cilia and cilia-generated flow image processing and analysis

Bead flow tracing, ciliary length and motion were determined using Fiji [38] with the following functions: Stack function was applied to bead propagation movies and saved images were opened in Microsoft Office™ Powerpoint for manual overlay and isolation of the area in focus. Live cilia imaging sequences were screened for the display of full-length cilia to manually measure length. The beating angle was determined by scrolling through the sequence and identifying the positions during the beating. Phase was visualized by determining the period and color-coding of cilia position during a single active recovery stroke. Phase synchrony was quantified from values of pixel grey scales of kymographs obtained from the cilia motion recordings. For human nasal scrapes, an average of 10 different recordings was used for each individual. For mouse trachea, we measured 261 cilia for wildtype and compared them to 56 of *Cdkl5* KO mice. For length measurement of murine ependymal cilia, we measured 145 in wildtype mice, 256 in *Cdkl5* KO mice, and 236 for *Yes1*$^{+/mt}$ mice. For angle measurement of ependymal cilia motion, we measured $n=72$ bundles for wildtype, 51 bundles for *Cdkl5* KO mice, 107 bundles for *Yes1*$^{+/mt}$ mice. For quantitative assessment of phase synchrony, greyscale values of $n=12{,}125$ pixels were determined for controls, $n=19{,}834$ were used for patient 1, and $n=19{,}731$ for patient 2. Statistical comparison was conducted using two-tailed *t* test as the data was normally distributed. Measurement results are deposited in the Data summary table (Online Resource 1).

Modeling fluid dynamics for volumetric CSF-flow analysis

Geometries of the ventral part of the v3V of wildtype and *Cdkl5* KO mice were reconstructed from MRI data. Background intensity was adjusted and volume segmentation was retrieved automatically using Slicer 4.10 [11]. Reasonable smoothing was considered due to the limited spatial resolution of the MRI. The lattice Boltzmann method (Palabos 2.0, http://www.palabos.org/) was then used for studying the volumetric flows inside the ventricles. The walls were assumed to be rigid and non-slip, and an extrapolation method was adopted to treat curved boundaries. To generate flow, uniform velocity profiles with a physiologically reasonable value of 300 µm/s were applied at the inlet plane. This value was chosen as it corresponds to the velocity of cilia-generated flow in the anterior part of the ventricle. A constant pressure was specified at the outlet plane for reference. The kinetic viscosity of the CSF was 6.959e-7 m^2/s, the same as that for water at 37 °C. About 10 million lattices (or computational nodes) were used for every case so that all flow details were resolved. Flow features, such as velocity distributions were obtained and post-processed with ParaView 5.4 (https://www.paraview.org/).

Electron microscopy of cilia ultrastructure

Murine trachea and brain third ventricle tissue samples were fixed overnight in 2.5% glutaraldehyde, 2% paraformaldehyde in 0.1 M sodium cacodylate buffer pH7.4. Samples were then washed in buffer several times and post-fixed with 1% osmium tetroxide with 0.8% potassium ferricyanide in cacodylate buffer. Fixed tissue was then dehydrated through an ethanol series, transitioned to propylene oxide and embedded in Poly/Bed 812 epoxy resin. Ultrathin sections were generated and stained with methanolic uranyl acetate and examined in a Hitachi H-7650 transmission electron microscope operating at 80 kV.

Protein–protein interactome analysis

LENS software for network analysis finds the shortest paths in the human interactome that connect each of the genes being analyzed ('candidate genes') to one or more of the remaining candidate genes [17]. Known protein–protein-interactions (PPIs) were compiled from HPRD (Human

Protein Reference Database) and BioGRID (Biological General Repository for Interaction Datasets) [15], and novel PPIs were predicted by applying the HiPPIP algorithm [15]. [17] HiPPIP computes features of protein pairs such as Gene Ontology annotations, genomic location of the genes, gene expression, and classifies the pairwise features as interacting or non-interacting using the random forest model and is deemed highly accurate [5, 15]. Each protein (say M_1) was paired with every human protein (N1, N_2,…N_n), and each pair was evaluated with the HiPPIP model. The protein pairs that received a score > 0.5 from the model were treated as novel computationally predicted PPIs; this threshold indicated high-confidence PPIs according to thorough computational evaluations [15] and experimental validations [15, 20, 21].

Functional enrichment analysis: 184 genes associated with epilepsy (specifically, 32 different traits associated in some way with epilepsy including terms such as *epilepsy*, *generalized epilepsy*, *response to valproic acid in genetic generalized epilepsy*, etc.) were curated from the GWAS catalog (https://www.ebi.ac.uk/gwas/) [20]. The list of 165 cilia genes was curated from literature by prioritizing the genes based on their association with cilia [35]. This list includes IFT proteins, BBS proteins, transition zone proteins, ciliary membrane proteins, and proteins restricted to motile cilia. Mouse genes associated with seizure phenotypes, hydrocephalus and abnormal brain ependymal phenotypes were retrieved for interactome analysis by querying Mammalian Phenotype Ontology (http://www.informatics.jax.org/vocab/mp_ontology) [40] using the 'batch query' function in MGI Database. Gene Ontology Biological Process and Reactome Pathway enrichments were computed using WebGestalt (http://www.webgestalt.org/) [25]. WebGestalt computes the distribution of genes belonging to a particular functional category in the input list and compares it with the background distribution of genes belonging to this functional category among all the genes that belong to any functional category in the database selected by the user. Statistical significance of functional category enrichment was computed using Fisher's exact test, with Benjamini–Hochberg multiple test correction, with FDR-corrected p value < 0.05 considered to be significant.

Analysis of CDKL5 evolutionary sequence conservation

Molecular evolutionary analysis was conducted using Clustal Omega Multiple Alignment Tool https://www.ebi.ac.uk/seqdb/confluence/pages/viewpage.action?pageId=54646455 with accession numbers: AGC12987.1 for the *Chlamydomonas reinhardtii* homolog LF5, NP_001019795.1 for *Mus musculus* Cdkl5 and NP_003150.1 for *Homo sapiens* CDKL5. Sequence homology was determined using BlastP (https://blast.ncbi.nlm.nih.gov/Blast.cgi). The location of specific domains was determined using Interpro [13].

Results

To investigate the role of CDKL5 in regulating motile cilia length and motility, we recruited two CDD patients with informed consent, a female (P1) heterozygous for a *CDKL5* splicing defect mutation (c.65-1 G > A) and a male subject (P2) hemizygous for a *CDKL5* frameshift mutation (p.Val659Glyfs*23) (Table S1). Both patients began having seizures at 5–6 weeks of age, with up to 8 seizures per day that are intractable and unresponsive to treatment. Both exhibited global developmental delay with static encephalopathy, cortical visual impairment, hypotonia and communication only via nonverbal vocalization (detailed clinical history in Supplemental Information). Nasal scrapes were conducted from the two CDD patients and also from five control subjects to obtain respiratory epithelial tissue lined with motile cilia mediating airway mucociliary clearance. Tissues were fixed and immunostained with a CDKL5 antibody to examine the expression of CDKL5 in the nasal epithelia. Live tissue was also examined for ciliary motion using videomicroscopy. In parallel to the analysis of the human airway epithelia, we obtained tracheal multiciliated cells from the *Cdkl5* knockout mice to examine the impact of *Cdkl5* deficiency on motile cilia in the mouse airway epithelia.

CDD patient airway cilia show lengthening with abnormal motion

Immunostaining with a CDKL5 antibody showed CDKL5 localization in the ciliary axoneme and basal body of the control subject (Fig. 1a). However, such staining was not observed in the CDD patient samples, confirming deficiency of CDKL5 (Fig. 1b). High-speed videomicroscopy showed robust cilia motion (Online Resource 2). Significant cilia lengthening was noted in both patients when compared to healthy control subjects (Fig. 1c). We further investigated cilia beating characteristics by using still images from these video recordings of control nasal cilia to track the positions of neighboring cilia at the beginning and end of the active versus recovery stroke. In the control subject, cilia are found upright at the beginning of the active stroke and synchronously bend forward to the transition into the recovery stroke (Fig. 1d). This phase synchrony persisted during subsequent strokes as shown by extraction and color-coding of cilia positions at three different time points during each stroke (Fig. 1e). In contrast, in CDD patients, there was a loss of phase synchrony with cilia found at different positions at different times during the stroke (Fig. 1f,g). This

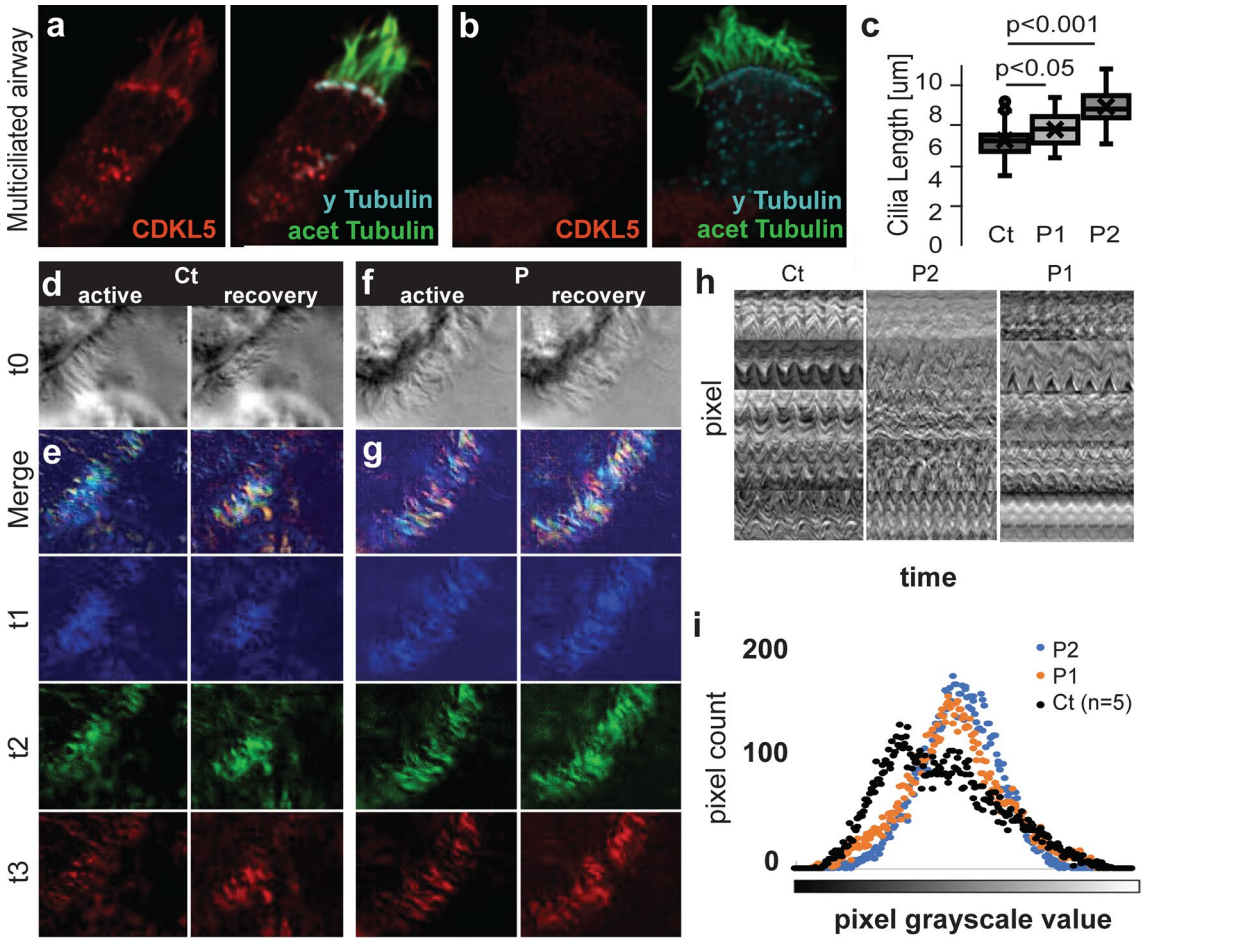

Fig. 1 Length and beating of motile cilia is altered in CDKL5 deficiency. **a** Immunostaining of CDKL5 in human nasal epithelia reveals ciliary localization seen in controls (Ct) **b** is absent in CDD-patients. **c** Motile cilia lengthening is observed in the female patient (P1) and the male patient (P2). **d** Still images (t0) show an upright position at the beginning of the active stroke and synchronously bend forward at the beginning of the recovery stroke. **e** This is illustrated in more detail as color coding of stroke progression (time intervals t1-t3). **f**, **g** Motile cilia of CDD patients are in an upright position while neighboring cilia are bend forward at the same time. **h** Kymographs of different cilia bundles show a zigzag pattern for synchronously beating motile cilia of healthy controls ($n=5$) while a more averaged grey scale is observed for the patient cilia. **i** Pixel grey scale distribution confirms greyscale intensity of kymographs is divided between two values in controls while a single peak is observed for average greyscale in both patients

can be clearly observed via kymographs of cilia motion (Fig. 1h). Quantification of kymograph greyscale showed a biphasic graph reflecting the zig-zag pattern of synchronized cilia in controls, while CDD patient yielded a single peak of the average greyscale in disorganized cilia motion (Fig. 1i). Together these findings showed in CDD patients significant cilia lengthening accompanied by abnormal cilia motion with the loss of phase synchrony.

Cdkl5 knockout mouse airway cilia show lengthening with abnormal motion

Tracheal epithelia of control mice were examined for Cdkl5 with confocal immunomicroscopy. This showed Cdkl5 localization in the axoneme of motile cilia in the tracheal epithelia of wildtype mice (Fig. 2a), but no staining was observed in the multiciliated tracheal epithelia of the *Cdkl5* KO mice (Fig. 2b). Motile cilia in the *Cdkl5* KO mice showed significant lengthening compared to controls (Fig. 2c). Videomicroscopy and analysis of cilia motion showed phase synchrony in the control mice, but not in the *Cdkl5* KO mice, similar to findings in the CDD patients (Fig. 2d). Analysis of the tracing of ciliary motion showed uniform cilia beating orientation in wildtype mice, but in the *Cdkl5* KO mice, cilia beating direction was less organized (Fig. 2e). Electron microscopy showed no cilia axonemal ultrastructural abnormalities in the *Cdkl5* KO mouse tracheal epithelia (Fig. 2f), although occasional membrane protrusions or fusion of neighboring cilia (Fig. 2g) were observed even as the axonemes remained distinct. Overall,

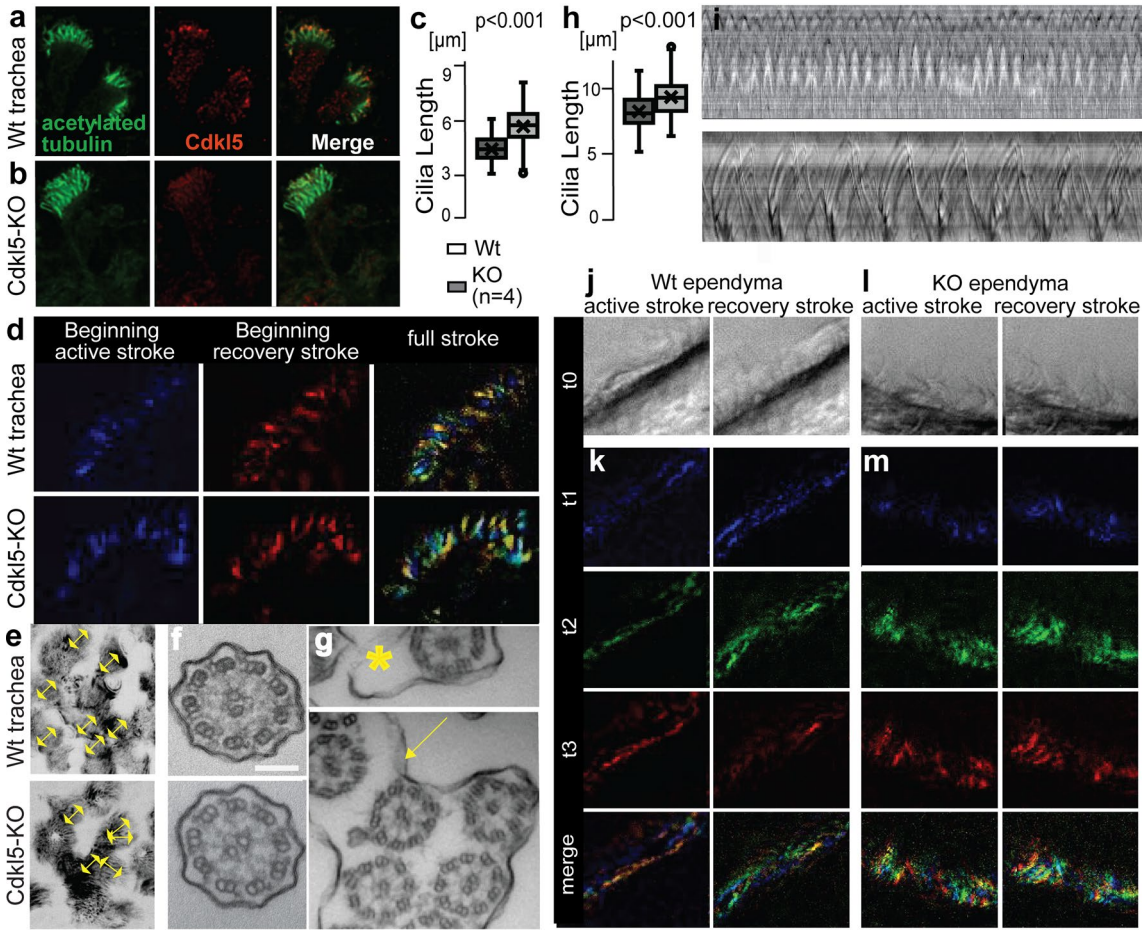

Fig. 2 Cdkl5 regulates motile cilia length and beating. **a** Immunostaining of Cdkl5 in murine airway epithelia reveals ciliary localization **b** and its absent in *Cdkl5* KO mice. **c** Airway motile cilia of *Cdkl5* KO mice are longer. **d** Temporal color coding for stroke progression reveals synchrony observed for wildtype (WT) motile cilia beating is absent in *Cdkl5* KO mice. **e** Projection of top-view videos of cilia motion shows uniform orientation of cilia beating in wildtype trachea is lost in *Cdkl5* KO mice. **f** Electron micrographs show no gross abnormalities of ciliary axonemes in *Cdkl5* KO mice, but occasional ciliary membrane abnormalities such as **g** protrusions and fusion between neighboring cilia. **h** Brain motile cilia of *Cdkl5* KO mice are lengthened. **i** Uniform zigzag pattern in kymographs of cilia motion shows phase synchrony for motile cilia of wildtype controls absent from *Cdkl5* KO mice. **j** Still images show cilia in an upright position at the beginning of the active stroke and synchronously bending forward at the beginning of the recovery stroke in wild-type mouse. **k** This is better illustrated with the additional panels showing color coding of stroke progression. **l** In contrast, motile cilia of *Cdkl5* KO mice are in an upright position while neighboring cilia are bending forward at both the active and recovery stroke, **m** which is evident with the1 color coding of stroke progression

these findings indicate the function of CDKL5 in the regulation of cilia length and motion is conserved in human and mouse airway cilia.

Cdkl5 regulates cilia length and motion at the brain ventricular surface

Using the *Cdkl5* KO mice, we further investigated the impact of Cdkl5 deficiency on motile cilia in the ependymal epithelia interfacing between brain tissue and CSF in the ventricular system. Similar to the motile cilia in the airway, motile cilia lengthening was observed and robust cilia motility (Online Resource 3) was preserved in the *Cdkl5* KO mouse brain ependyma (Fig. 2h). While kymographs of wildtype control mice showed the standard zigzag pattern indicating synchrony of cilia beating, kymographs of *Cdkl5* KO mice showed beating of cilia occurs out of phase (Fig. 2i). This is also evident with analysis of ciliary motion (Fig. 2j) with color coding of cilia positions during stroke progression (Fig. 2k). This showed the disruption of phase synchrony in the *Cdkl5* KO mouse ependyma such that cilia within a bundle had variable positions during the active and recovery strokes, while in the wildtype ependyma they were more coordinated (Fig. 2l,m). These findings indicate Cdkl5 is required for regulating brain ependymal cilia phase synchrony, similar to findings obtained for the respiratory cilia.

Cdkl5 deficiency alters flow pattern in v3V to block cilia-mediated fluid inflow

We previously showed ependymal cilia generated a highly organized pattern of flow that can mediate directional transport in the ventral third ventricle (v3V) in the ventral third ventricle (v3V) [10]. To determine the impact of abnormal cilia motion on such cilia-generated transport, explants of the v3V (Fig. 3a) were placed in a medium containing fluorescent beads to allow tracking and mapping of the pattern of fluid flow at the ependymal surface. In wild-type explants, we observed the stereotypic pattern with an inflow stream at the narrow anterior duct and an outflow stream at the posterior duct (Fig. 3b,c, Online Resource 4). Tracing cilia beating orientation showed cilia beating polarity was uniform and aligned with the direction of fluid flow, predicting directional transport of substances along the ependymal surface of the ventricular system (Fig. 3d).

To investigate fluid turnover or clearance in the v3V, a micropipette was used to release a bolus of fluorescein isothiocyanate (FITC)-dextran to mimic freshly delivered CSF. In the wildtype mouse v3V, efficient clearance was observed, with the tracer rapidly spreading from the anterior duct across the anterior and dorsal surface of the v3V (Fig. 3e, Online Resource 5). Analogous analysis of the *Cdkl5* KO mouse v3V revealed that the flow map (Fig. 3f,g) showed a circular flow stream or whirl at the anterior duct that blocked cilia-mediated inflow into the v3V (Online Resource 4). Tracing of cilia orientation showed random cilia beating orientation (Fig. 3h). The FITC-dextran did not spread, but stagnated at the site of injection at the anterior duct, demonstrating clearance was effectively blocked (Fig. 3i, Online Resource 5). Further computational modelling of fluid dynamics points to a crucial role for cilia-generated flow rather than bulk flow in mediating clearance in the v3V (Fig. SI2).

As electron-dense structure known as the basal foot anchor the ciliary basal bodies to align cilia polarity in other multiciliated tissues [47], we further conducted electron microscopy to examine basal foot orientation in the v3V ependyma. Surprisingly, multiple electron-dense masses were observed with each basal body, obscuring the use of basal feet for determining cilia polarity (Fig. SI3).

Motile cilia defects and abnormal ciliary motion in *Yes1* mutant mice

Given sequence conservation in CDKL5 between *Chlamydomonas*, mice, and man is restricted to the kinase domain (Fig. SI4), this suggests the kinase function may be pivotal in the regulation of motile cilia function. To investigate this further, we examined ependymal cilia in mice harboring L1435P missense mutation in the kinase domain of another epilepsy-related serine-threonine kinase *Yes1* [16, 24]. Interestingly motile cilia in the v3V of heterozygous *Yes1*$^{+/mt}$ mice showed significant lengthening (Fig. 4a). Cilia motion analysis showed the increased angle of cilia beating in both the *Yes1*$^{+/mt}$ and *Cdkl5* KO mouse ependyma (Fig. 4b). Importantly, analysis of v3V flow maps showed similar to the *Cdkl5* KO mice, pronounced whirls blocking the inflow into the v3V (Fig. 4c).

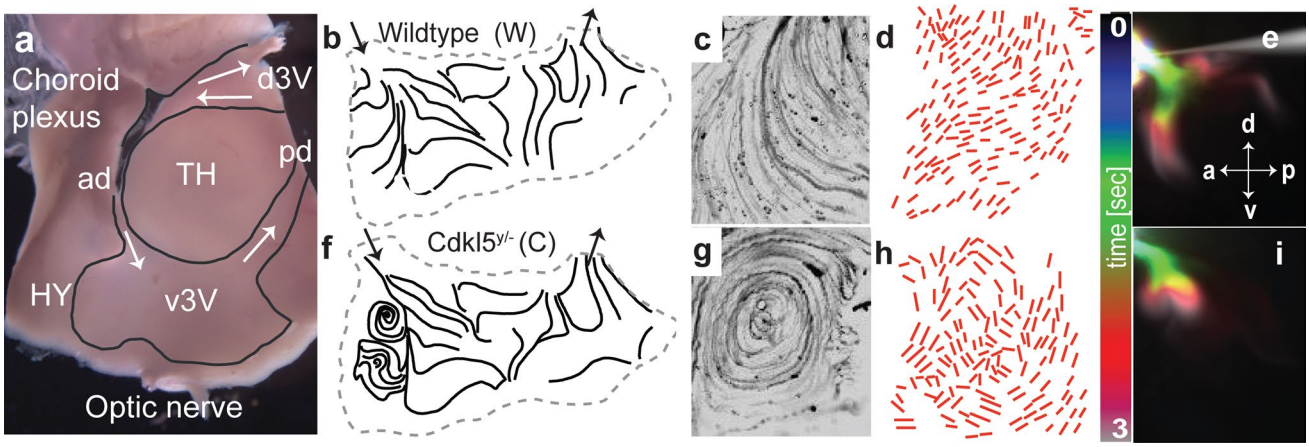

Fig. 3 Mispatterned cilia-driven flow blocks fluid transport in *Cdkl5* KO mice. **a** Explant with dorsal (d3V) and ventral third ventricle (v3V, black outline) facing the hypothalamus (HY) and Thalamus (TH) and cilia-generated flow (white arrow) via the anterior (ad) and posterior duct (pd). **b** Flow maps show tracing of cilia-generated flow. **c** Tracing of fluorescent beads being transport from into the anterior v3V with the surface flow. **d** Cilia-beating direction underlying the surface flow. **e** Time-resolved color-coding of distribution of FITC-dextran following injection into ad. **f** Flow maps are altered in *Cdkl5* KO mice **g** with an expansive whirl appearing below the anterior duct, **h** arising from misoriented cilia bundles and **i** preventing inflow of fluid from the anterior duct clearing the anterioventral surface of v3V

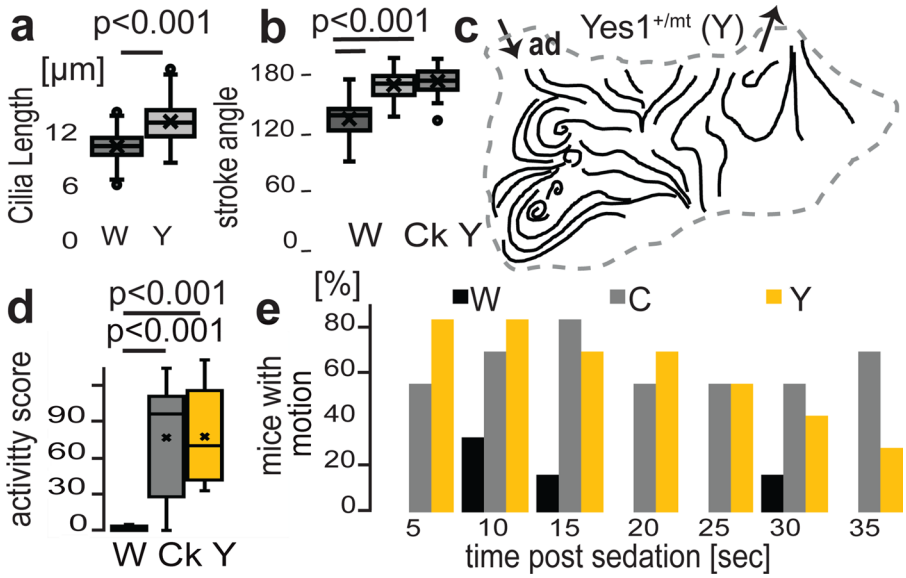

Fig. 4 Flow is also regulated by Yes1, another epilepsy-related kinase. **a** Cilia lengthening is observed in *Yes1*$^{+/mt}$ mice. **b** The angle of cilia beating in Yes1 is similarly increased in *Yes1*$^{+/mt}$ mice as in *Cdkl5* KO mice. **c** Flow maps reveal the presence of the flow-blocking whirls below the anterior duct. **d** Seizure-like motion after anesthesia induction shows greatly increased scores in the *Yes1*$^{+/mt}$ and *Cdkl5* KO mice. *W* wildtype, *C* hemizygous *Cdkl5* KO, *Y Yes1*$^{+/mt}$ mice. **e** Incidence of any involuntary motion over time shows prolonged susceptibility

Increased seizure susceptibility in *Cdkl5* KO and *Yes1*$^{+/mt}$ mice

Our findings indicate the cilia-generated active blockage of flow is critical for CSF-turnover in the v3V. Thus flow blockage impairing homeostatic balancing of the brain would be expected to increase seizure susceptibility [19, 42] (Fig. SI1). However, as spontaneous seizures are rare in the *Cdkl5* KO mice [26, 45], this suggests under normal conditions, the mouse brain may retain sufficient homeostatic balance despite the flow blockage. To test whether the cilia-generated flow blockage when combined with experimentally induced CSF homeostatic imbalance might be insufficiently cleared, we established a protocol to assay mice for susceptibility to isoflurane-induced seizure-like activity (Fig. SI5). Isoflurane, an anesthetic that induces lactate release into the CSF [18], have been described to cause seizure in patients [48, 53]. Indeed seizure-like activity was observed in *Cdkl5* KO mice and *Yes1*$^{+/mt}$ mice upon anesthesia induction with isoflurane (Fig. 4d). While wildtype mice showed only mild twitching of the limbs and neck shortly after sedation, *Cdkl5* KO mice and *Yes1*$^{+/mt}$ mice showed jerking and severe convulsions that persisted for a much longer time period (Fig. 4e). These findings indicate serine-threonine kinases that modulate motile cilia and the patterning of cilia generated flow may contribute to increased seizure susceptibility.

Cdkl5 deficiency restricted to multiciliated cells is sufficient to cause flow blockage

As *Cdkl5* is expressed not only in the multiciliated ependymal cells but also in neurons and other cell types in the brain, we further investigated whether CDKL5 deficiency in the ependyma alone is sufficient to generate the v3V inflow obstruction seen in the *Cdkl5* KO mice. *Cdkl5* deletion targeted to the brain ependyma was carried out using a *Cdkl5* floxed allele (*Cdkl5*$^{y/fl}$) in conjunction with a tamoxifen-inducible *FOXJ1* promoter-driven Cre (FOXJ1Cre^{ERT}) [36, 44]. In the absence of FOXJ1Cre^{ERT} induction, analysis of the v3V flow map revealed normal patterning of flow in the *Cdkl5*$^{y/fl}$ mice (Fig. 5a), but following tamoxifen induction of Cre, we observed the same flow blockage at the v3V inflow as seen in the *Cdkl5* KO mice (Fig. 5b), confirming CDKL5 deficiency in the ependymal cells alone is sufficient to replicate the v3V inflow blockage seen in the *Cdkl5* KO mice.

Mispatterning of cilia beating in the brain is a novel type of ciliopathy

Our finding that the *Cdkl5* KO and *Yes1*$^{+/mt}$ mice both show similar cilia motility disturbances and blockage of cilia generated inflow into the v3V support a role for motile cilia defects in the increased susceptibility to anesthesia-induced seizure-like activity observed in these mice. To investigate if the motile cilia disturbances alone are sufficient to cause increased susceptibility to anesthesia-induced seizure-like activity, we examined mice with haploinsufficiency in *Foxj1*, a master transcriptional regulator of motile ciliogenesis [28]. While homozygous *FoxJ1* KO mice fail to form cilia in the brain ependyma and succumb to hydrocephalus, heterozygous *Foxj1* KO mice (*FoxJ1*$^{\pm}$) are adult viable and grossly normal [29]. Their brain ependymal epithelium is lined with multiciliated cells with the robust cilia-generated flow (Online Resource 6).

We retrieved v3V of the *FoxJ1*$^{\pm}$ mice and mapped the cilia-generated flow. Flow maps showed the same striking whirl below the anterior duct of the v3V (Fig. 6c), indicating blockage of inflow from the anterior duct. This was

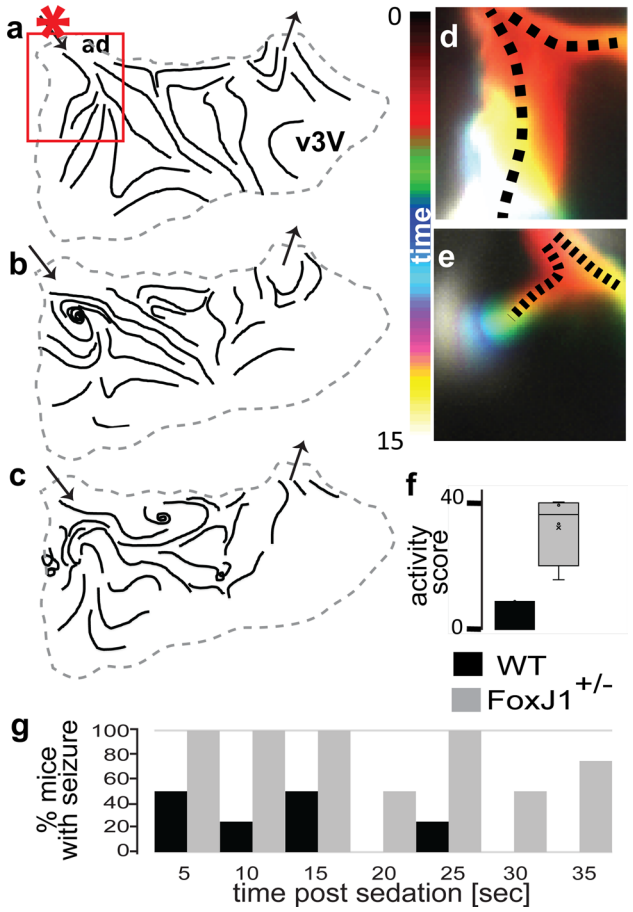

Fig. 5 Cilia-generated flow blockage is a novel type of ciliopathy. **a** Flow maps of *FOXJ1Cre*^{ERT}:*Cdkl5*$^{y/fl}$ mice shows normal patterning without tamoxifen and **b** flow whirls with tamoxifen-induced activation of the Cre recombinase. **c** 4 weeks old *FoxJ1*$^{\pm}$ mice show whirl-like flow abnormalities **d** with normal fluid clearance in wildtype littermates (**e**) and flow blockage in *FoxJ1*$^{\pm}$ KO mice (**e**). **f** Five-weeks old wildtype littermates showed occasional twitching of limbs and neck during anesthesia with isoflurane whereas more severe twitching and convulsions were observed in *FoxJ1*$^{\pm}$ mice. **g** This activity persists over a longer duration following sedation

confirmed by tracking cilia-mediated inflow of FITC-dextran released above the wall of the anterior duct. While wildtype mice showed a rapid spread of the injected tracer along the v3V surface (Fig. 6d), in the *FoxJ1*$^{\pm}$ mice the tracer remained near the injection site at the v3V inlet, confirming blockage of inflow at the anterior duct (Fig. 6e). Assessment of seizure-like activity following sedation with isoflurane showed the *FoxJ1*$^{\pm}$ mice with increased convulsions (Online Resource 7, Fig. 6f) and these were much longer in duration, findings similar to those obtained in the *Cdkl5* KO and *Yes1*$^{+/mt}$ mice (Fig. 6g). In contrast, wildtype littermates showed only occasional twitching of limbs or neck (Online Resource 8). We conclude the cilia-generated flow blockage is sufficient to cause seizure susceptibility, supporting the essential role of motile cilia defects in causing increased seizure predisposition. These findings suggest some seizure disorders may be a new class of ciliopathy involving motile cilia defects in the brain ependyma.

Ependymal ciliary rootlets form highly structured anchoring meshwork

To investigate the possible underlying cause for the abnormal ciliary beating polarity and resulting flow obstruction, we investigated the organization of the ciliary rootlet meshwork in the v3V. Studies in the Xenopus multiciliated epidermis have shown the rootlet meshwork regulates directional cilia beating by organizing the positioning of basal bodies and their linkage to the actin cytoskeleton [42]. Confocal microscopy using antibodies to γ-tubulin for visualizing the basal bodies, and rootletin for delineating the rootlet meshwork showed the basal bodies in the v3V ependyma are encased in a dense meshwork of rootletin-positive fibers. Individual rootelin fiber can be seen projecting from the meshwork to the cell surface, meeting a similar rootelin fiber in the opposing cell (Fig. 6a–d). The rootelin fibers also appear to form a thin sheath encasing the nucleus (Fig. 6d). Importantly, these rootelin meshworks are highly polarized at the anterior duct of the v3V. The long axis is aligned with the direction of cilia beating and cilia-mediated flow (Fig. 6e), supporting a role for the rootlet meshwork in specifying cilia beating orientation.

Polarized anchoring meshwork specifies regional cilia beating polarity

To investigate whether their changes in the rootlet meshwork may be associated with the altered motile cilia beating polarity in the v3V of *Cdkl5* KO and *Yes*$^{+/m}$ mice, we conducted confocal immunomicroscopy of the v3V ependyma in both mutant mice. This analysis showed both mutants had rootlet meshwork with a more rounded configuration as compared to the eccentric or oval shape meshwork in wildtype mice (Fig. 7a–c). This was demonstrated by quantifying the aspect ratio of the rootlet meshwork. The more rounded rootlet meshwork in the mutants is associated with the whirl obstructing inflow into the v3V inlet (Fig. 3).

As motile cilia anchoring via the rootlet meshwork also has been shown to involve ciliary adhesions analogous to focal contacts, we further investigated the distribution of Pak2, a p21 kinase with critical roles in the regulation of focal adhesions. Pak2 is also a downstream effector of Yes1 [21, 43, 52] and also of Cdkl5 via regulation by Rac1 [8]. Little or no Pak2 immunostaining was observed in the wild-type mouse v3V ependyma (Fig. 7d). However, in both the *Cdkl5* KO and *Yes1*$^{+/mt}$ mice, we observed prominent Pak2 localization in a fiber-like meshwork encasing the basal bodies (Fig. 7e,f).

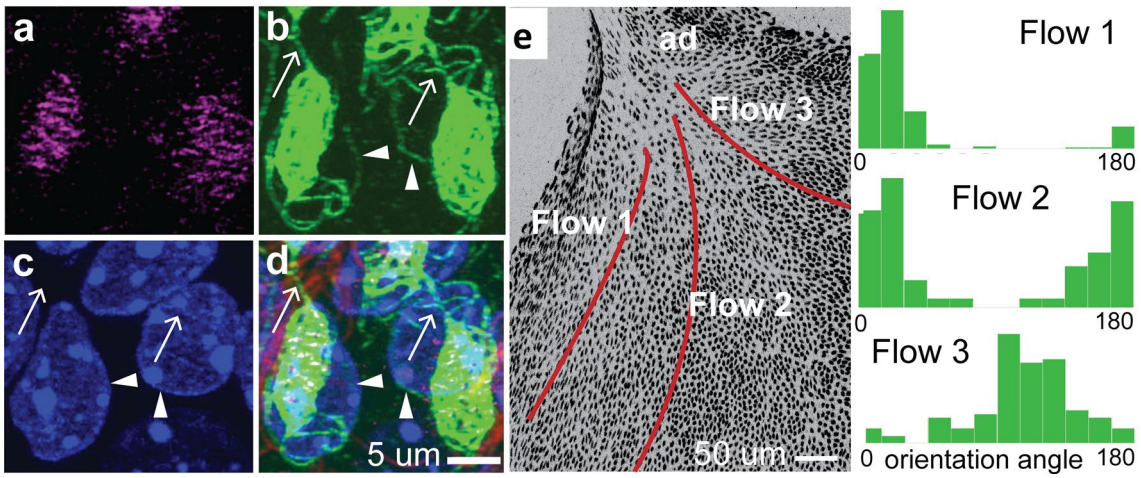

Fig. 6 Polarization of cilia anchoring meshworks correlate with the flow direction. **a–d** Immunostaining shows basal bodies are embedded in a meshwork of rootletin-stained fibers that wrap around the nucleus (arrowhead) and interconnect between cells (arrow). Bar = 5 µm. (**e**) Immunostaining for rootletin shows an eccentric structure with the long axis pointing in the direction of cilia-generated flow (indicated by red lines). Bar = 50 µm. The directionality of the long axis of rootletin-positive structures is aligned with the direction of flow

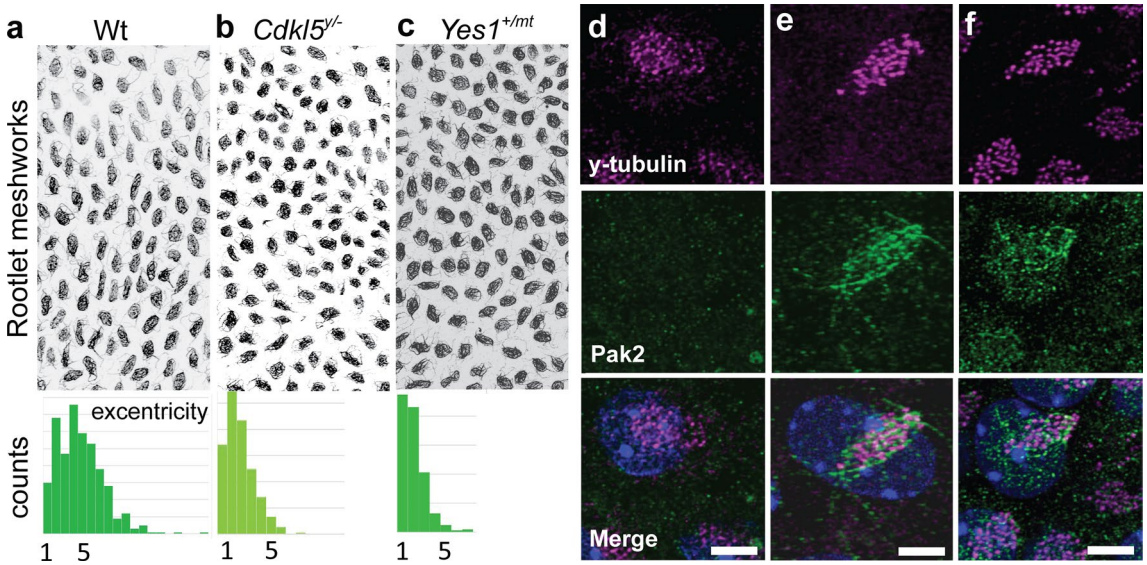

Fig. 7 Kinases regulate the polarized cilia anchoring structure. **a-c** In wildtype mouse ependyma (**a**), rootletin-stained structures are eccentric while roundess is increased in **b** *Cdkl5* KO and **c** *Yes1*$^{+/mt}$ mice. **d** Immunostaining reveals little or no Pak2 staining in the ependymal cells of wildtype (WT) mice, and colocalization with fibrous structures above the nucleus (blue) in *Cdkl5* KO (**e**) and *Yes1*$^{+/mt}$ **f** multiciliated ependymal cells. Bar = 3 µm. **g** Scheme shows organized cilia motion in wildtype cells (**h**) with interconnected polarized meshworks of rootlet fibres. **i** In the epilepsy-associated ciliopathy, cilia motion is destabilized **j** with disrupted rootlet meshwork together with ectopic Pak2 localization

Although it was not possible to pursue Pak2 and rootelin co-immunolocalization (given the lack of antibodies of different species or isotypes), the Pak2 meshwork is very reminiscent of those observed with the rootletin antibody and is likely to be localized in the rootelin meshwork (Fig. 6a–d). Together these findings suggest Cdkl5, together with other kinases may regulate cilia beating orientation through changes in the organization of the ciliary rootlet meshworks and thus pattern cilia-mediated flow in the brain ependymal surface.

CDKL5/YES1/PAK2 interactome recovers seizure-related genes

To investigate the possible larger genomic context for the modulation of motile cilia and seizure susceptibility, we assembled a protein–protein interaction PPI network (interactome) with CDKL5, YES1 and PAK2, the three kinases identified to have a significant impact on ependymal cilia function (Fig. SI6). The PPI network comprised 172 genes. From this interactome, we recovered five additional cilia proteins (CDC42, NPHP1, GAS8, CETN1, PDCD6IP), four proteins associated with ependymal defects (CDC42, BICD2, GAS8, PDCP6IP), three of which are cilia proteins, and 13 proteins associated with hydrocephalus (CETN1, GAS8, PTEN, SLC9A3R1, DLG4, PDCD6IP, CASP3, TP53BP2, GFAP, GAB1, SOCS7, BICD2, CDC42) (Online Resource 9). Also recovered were ten additional proteins with seizure phenotypes in mice (PTEN, TYRO3, DST, GFAP, BRAF, RASA1, FYN, APP, SYN1 and FMR1) (nodes with black outlines in Fig. SI6), three with confirmed association with human epilepsy (nodes with black dots in Fig. SI6). Also recovered in the interactome is PTK2, which encodes focal adhesion kinase. PTK2 is not only a YES1-interactor and a known downstream effector of PAK2 [32], but was also shown to regulate cilia orientation in the *Xenopus* epidermis [2]. Many relevant pathways such as actin filament organization, small GTPases mediated signal transduction, cell-substrate adhesion, the establishment of tissue and cell polarity are statistically enriched in the interactome (Online Resource 9). Together these findings support CDKL5, YES1 and PAK2 being part of a kinase-network that regulates cytoskeletal organization and the specification of cilia polarity with functional impact on hydrocephalus and epilepsy (Fig. 8).

Discussion

We showed CDKL5, an evolutionarily conserved kinase associated with the neurodevelopmental disorder CDD, has retained the ancient function of regulating motile cilia. Reminiscent of observations in the *Chlamydomonas lf5* mutants [43], CDD patients and the *Cdkl5* KO mice showed cilia lengthening and abnormal cilia motion in the airway epithelia. Brain ventricular epithelia of the *Cdkl5* KO mice also showed ependymal cilia lengthening and abnormal cilia motion. Flow mapping revealed distinct alterations in the pattern of cilia-generated flow in the v3V, with flow obstruction observed in the v3V that indicates blockage of CSF circulation. Importantly, increased seizure-like activity was observed in *Cdkl5* KO mice and other mutant mice exhibiting similar cilia-generated flow blockage at the v3V inlet.

Cilia generated flow blockage in the brain ventricles as a mechanism of epilepsy

Evidence for a functional link between the patterning of cilia-driven flow in the brain and seizure susceptibility was demonstrated with the analysis of the *Cdkl5* KO, *FoxJ1*$^{\pm}$, and *Yes1*$^{+/mt}$ mice. They all exhibited an increase in anesthesia-induced seizure-like activity in combination with the stagnation of cilia-driven inflow into the v3V. This flow blockage predicts failure in CSF clearance that would lead to homeostatic imbalances in the brain tissue and thus promote seizure-like activity [19, 42]. In the context of this cilia-based seizure model, the rarity of spontaneous seizures in the *Cdkl5* KO mice may reflect the efficacy of diffusion-mediated CSF equilibration in the smaller size mouse brain that is not possible in the larger size human brain. Consistent with this, increased seizure susceptibility in *Cdkl5* KO mice becomes apparent upon exposure to isoflurane that induces imbalances in CSF homeostasis [18]. This would also predict animal models with the larger brain such as pig or sheep may provide a better context to model seizures associated with cilia-driven flow blockage.

As the sequence conservation of CDKL5 is restricted to the kinase domain [43] (Fig. SI2), this suggests the kinase activity of CDKL5 may be pivotal to the modulation of motile cilia structure and function. Given the additional involvement of two other kinases, Yes1 and Pak2, in the ependymal flow obstructions, this would suggest cilia regulating kinases may comprise a new class of therapeutic targets for medication-resistant epilepsy.

Ciliary rootlet anchoring meshwork pattern cilia beating polarity and cilia mediated flow

We showed the cilia-driven flow blockage in the v3V arises from alterations in cilia beating orientation. This is associated with perturbation of the rootletin containing ciliary rootlet meshwork. Analysis of multiciliated Xenopus epidermis has shown the ciliary rootlets regulate the precise spacing of the basal body and the anchoring of the basal body to the actin cytoskeleton [50]. In mammals, the airway ciliary rootlets reach from the basal bodies into the cytoplasm and seem to be dispensible for cilia motion and mucociliary clearance whereas, in the photoreceptor cells of the retina, they form a nucleus-ensheathing structure shown to provide long-term structural integrity of the sensory cilium [51]. It seems the distinct features of the cilia-anchoring meshwork structure from different cell types are combined in the multiciliated ependyma, possibly explaining the unexpected finding of stereotypic patterning in v3V in wild-type animals [10] and its disruption in CDD.

Interestingly, basal body anchoring via rootlets to the actin cytoskeleton also requires ciliary adhesions containing

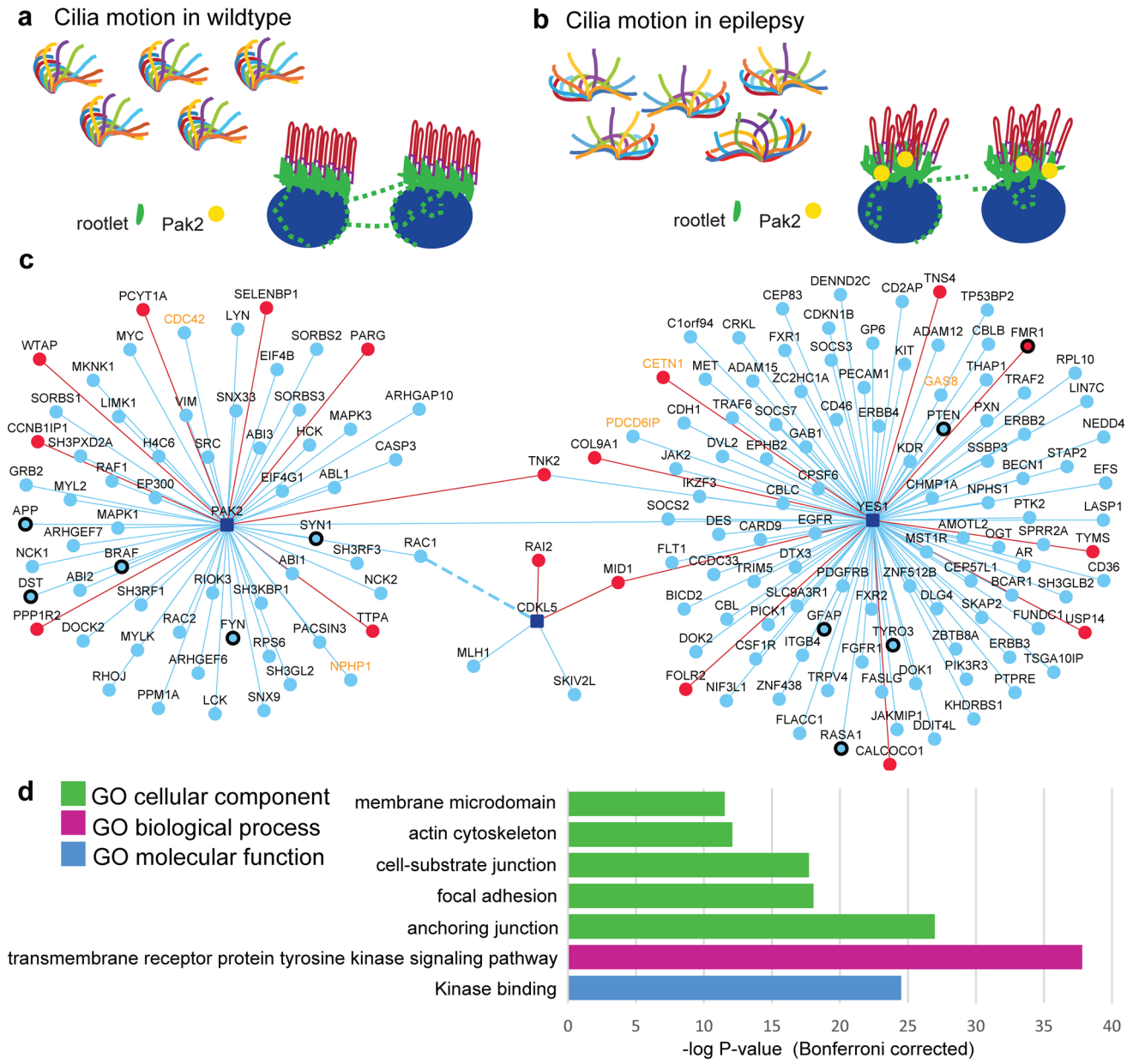

Fig. 8 Protein–protein interactome comprising CDKL5, YES1 and PAK2. **a** Scheme shows organized cilia motion in wild-type cells with interconnected polarized meshworks of rootlet fibres. **b** In the epilepsy-associated ciliopathy, cilia motion is destabilized with disrupted rootlet meshwork together with ectopic Pak2 localization. **c** An interactome was constructed comprising 172 genes, assembled based on known (blue) and novel (red nodes) protein–protein interactions (PPIs) of CDKL5, PAK2, and YES1 (light blue nodes/edges: known interactors/PPIs, red nodes/edges: novel interactors/PPIs). Five additional cilia proteins (labeled in yellow) were recovered including CDC42, NPHP1, GAS8, CETN1 and PDCD6IP. Of these, three are also associated with ependymal cilia defects (PDCD6IP, GAS8, CETN1, CDC42). Eight proteins in the interactome are associated with hydrocephalus in mice, including CETN1, GAS8, PTEN, SLC9A3R1, DLG4, PDCD6IP, CASP3, TP53BP2, GFAP, GAB1, SOCS7, BICD2 and CDC42. Ten additional proteins are associated with seizure phenotypes in mice (nodes with black outline) including: PTEN, TYRO3, DST, GFAP, BRAF, RASA1, FYN, APP, SYN1 and FMR1. GWAS analysis indicated three proteins are associated with human epilepsy (nodes with black dot): ARHGAP10 (benign childhood epilepsy with centro-temporal spikes), C12orf94 (generalized epilepsy), and FMR1 (associated with fragile × syndrome). FMR1 is also known to cause epilepsy in mice (node with black outline and dot). **d** Analysis of the interactome for GO Biological Process showed significant pathway enrichment related to actin filament and cytoskeletal organization, cell adhesion, and signal transduction pathways regulating these processes, supporting the important role of these genes in patterning ependymal cilia polarity and ependymal cilia mediated flow

components typically found in focal adhesions, such as paxillin, vinculin, and focal adhesion kinase [2]. Significantly, Pak2 which we found ectopically in the ciliary rootlets in the *Cdkl5* KO mouse ependyma is known to regulate focal adhesion turnover through phosphorylation of paxillin. Pak2 also has been observed to form signaling complex containing the Par3 polarity protein to direct cell polarity [4]. Hence perturbation of ciliary adhesions at the rootlet meshwork could be responsible for increased stroke angle, loss of phase synchrony and defects in tissue polarity of cilia beating in CDD. It could also account for the cilia lengthening via disturbance of the actin cytoskeleton known to have an important role in regulating ciliogenesis itself [22, 41]. We note actin is also known to play a critical role in regulating flagellar length in *Chlamydomonas* [9]. These findings suggest perturbations of the rootlet meshwork may underlie the observed v3V cilia-mediated flow obstruction.

Brain ependymal cilia defects describe a new class of ciliopathy

Ciliopathies, diseases mostly involving defects in non-motile primary cilia are well described to be associated with neurodevelopmental disorders such as Joubert syndrome, acrocallosal syndrome, among others [37]. We note primary cilia defects have also been reported for *Cdkl5* deficient cells in culture, suggesting *Cdkl5* may have a broader role in regulating ciliogenesis [6]. Consideration of motile cilia defects in ciliopathies has largely focused on sinopulmonary disease, primary ciliary dyskinesia (PCD). In PCD, mucociliary clearance deficits are observed, but hydrocephalus or seizure susceptibility is generally not noted. This suggests motile cilia dysfunction in PCD is fundamentally different from motile cilia disturbances seen in CDKL5 deficiency. In PCD, severe cilia motion defects are observed, typically immotile cilia or cilia with severe dyskinetic motion incapable of generating flow [27, 39]. In contrast, cilia motion in CDD is robust and generation of flow per se is preserved, but the pattern of flow is disrupted, with flow blockage observed at the v3V inflow. This is created by altered polarity of the rootlet meshwork causing misaligned motile cilia beating polarity. These findings suggest CDD is a novel type of ciliopathy characterized by misguidance of CSF-flow and not the generation of flow per se. Given our finding indicating blockage of cilia-mediated fluid inflow is sufficient to predispose to seizure, this suggests proper cilia-mediated CSF circulation in the brain ventricular system is critical for homeostatic balance, pointing to a novel mechanism in epilepsy. In the context of this model, the rarity of spontaneous seizures in the *Cdkl5* KO mice under normal conditions may reflect adequate diffusion-mediated equilibration in the smaller-sized mouse brain. However, upon isoflurane exposure, seizures may arise due to metabolite release induced by the anesthesia in the presence of the cilia-driven blockage of flow preventing their clearance [18].

Altogether, these studies point to a crucial role of motile cilia and its regulation by the cilia-anchoring meshwork in patterning CSF flow in the brain and determining seizure susceptibility. Together with findings from the PPI network, a broader role is indicated for motile cilia in a new class of ciliopathy associated with epileptic disorders.

Supplementary Information The online version contains supplementary material available at https://doi.org/10.1007/s00401-022-02463-y.

Acknowledgements We thank Dr Pete Lefebvre for advising about the initial idea that CDD might be a motile ciliopathy. We thank Dr Joe Zhou and Dr Chay Kuo for generously providing *Cdkl5*$^{fl/fl}$, *Cdkl5*$^{y/fl}$ and *FOXJ1Cre*^{ERT} mice, and supporting with advice.

Author contributions Conceptualization: CWL, RJF; Methodology: CWL, RJF, SMK, YW, MKG; Data collection: RJF, MY; Recruitment of CDD patients: JG, NHB; Data analysis: RJF, VSC, MY; Computational Data analysis: RJF, YW, KBK; Visualization: RJF, TNF, YW, MKG, CWL; Funding acquisition: CWL, SMK, RJF; Project administration: CWL; Supervision: CWL, RJF; Writing—original draft: CWL, RJF; Writing—review and editing: CWL, RJF, SMK, YW, KBK, MKG.

Funding German Research Foundation grant FA 1457/1-1 (RJF); National Institutes of Health grant NIH HL142788 (CWL); National Institutes of Health grant NIH HL132024-01 (CWL); National Institutes of Health grant NIH GM051293 (SMK); MKG's effort is supported by Department of Biomedical Informatics of University of Pittsburgh School of Medicine.

Data availability Raw data will be made accessible upon request.

Declarations

Conflict of interest The authors declare that they have no competing interests.

References

1. Amendola E, Zhan Y, Mattucci C et al (2014) Mapping pathological phenotypes in a mouse model of CDKL5 disorder. PLoS ONE. https://doi.org/10.1371/journal.pone.0091613
2. Antoniades I, Stylianou P, Skourides PA (2014) Making the connection: ciliary adhesion complexes anchor basal bodies to the actin cytoskeleton. Dev Cell. https://doi.org/10.1016/j.devcel.2013.12.003
3. Barbiero I, de Rosa R, Kilstrup-Nielsen C (2019) Microtubules: a key to understand and correct neuronal defects in CDKL5 deficiency disorder? Int J Mol Sci. https://doi.org/10.3390/ijms20174075
4. Boscher C, Gaonać-Lovejoy V, Delisle C, Gratton JP (2019) Polarization and sprouting of endothelial cells by angiopoietin-1 require PAK2 and paxillin-dependent Cdc42 activation. Mol Biol Cell. https://doi.org/10.1091/mbc.E18-08-0486
5. Buniello A, Macarthur JAL, Cerezo M et al (2019) The NHGRI-EBI GWAS catalog of published genome-wide association studies,

targeted arrays and summary statistics 2019. Nucleic Acids Res. https://doi.org/10.1093/nar/gky1120
6. Canning P, Park K, Gonçalves J et al (2018) CDKL family kinases have evolved distinct structural features and ciliary function. Cell Rep. https://doi.org/10.1016/j.celrep.2017.12.083
7. Canning P, Park K, Gonçalves J et al (2018) CDKL family kinases have evolved distinct structural features and ciliary function. Cell Rep 22:885–894. https://doi.org/10.1016/j.celrep.2017.12.083
8. Chen Q, Zhu YC, Yu J et al (2010) CDKL5, a protein associated with Rett syndrome, regulates neuronal morphogenesis via Rac1 signaling. J Neurosci. https://doi.org/10.1523/JNEUROSCI.1102-10.2010
9. Dentler WL, Adams C (1992) Flagellar microtubule dynamics in Chlamydomonas: cytochalasin D induces periods of microtubule shortening and elongation; and colchicine induces disassembly of the distal, but not proximal, half of the flagellum. J Cell Biol 117:1289–1298
10. Faubel R, Westendorf C, Bodenschatz E, Eichele G (1979) Cilia-based flow network in the brain ventricles. Science 353:176–178. https://doi.org/10.1126/science.aae0450
11. Fedorov A, Beichel R, Kalpathy-Cramer J et al (2012) 3D Slicer as an image computing platform for the quantitative imaging network. Magn Reson Imaging. https://doi.org/10.1016/j.mri.2012.05.001
12. Fehr S, Wong K, Chin R et al (2016) Seizure variables and their relationship to genotype and functional abilities in the CDKL5 disorder. Neurology. https://doi.org/10.1212/WNL.0000000000003352
13. Finn RD, Attwood TK, Babbitt PC et al (2017) InterPro in 2017-beyond protein family and domain annotations. Nucleic Acids Res. https://doi.org/10.1093/nar/gkw1107
14. Fuchs C, Trazzi S, Torricella R et al (2014) Loss of CDKL5 impairs survival and dendritic growth of newborn neurons by altering AKT/GSK-3β signaling. Neurobiol Dis. https://doi.org/10.1016/j.nbd.2014.06.006
15. Ganapathiraju M, Chaparala S (2016) Schizophrenia interactome: fully-labeled interactome network. npj Schizophr. https://doi.org/10.1038/npjschz.2016.25
16. Guo W, Shang DM, Cao JH et al (2017) Identifying and analyzing novel epilepsy-related genes using random walk with restart algorithm. Biomed Res Int. https://doi.org/10.1155/2017/6132436
17. Handen A, Ganapathiraju MK (2015) LENS: Web-based lens for enrichment and network studies of human proteins. BMC Med Genomics. https://doi.org/10.1186/1755-8794-8-S4-S2
18. Horn T, Klein J (2010) Lactate levels in the brain are elevated upon exposure to volatile anesthetics: a microdialysis study. Neurochem Int. https://doi.org/10.1016/j.neuint.2010.09.014
19. Jupp B, Williams J, Binns D et al (2013) Metabolic causes of epileptic encephalopathy. Epilepsy Res Treat. https://doi.org/10.1155/2013/124934
20. Karunakaran K, Ganapathiraju M (2020) Interactome of SARS-CoV-2/nCoV19 modulated host proteins with computationally predicted PPIs. Res Sq. https://doi.org/10.21203/rs.3.rs-28592/v1
21. Karunakaran KB, Chaparala S, Lo CW, Ganapathiraju MK (2020) Cilia interactome with predicted protein–protein interactions reveals connections to Alzheimer's disease, aging and other neuropsychiatric processes. Sci Rep. https://doi.org/10.1038/s41598-020-72024-4
22. Kim J, Lee JE, Heynen-Genel S et al (2010) Functional genomic screen for modulators of ciliogenesis and cilium length. Nature. https://doi.org/10.1038/nature08895
23. Leonard H, Junaid M, Wong K et al (2021) Exploring quality of life in individuals with a severe developmental and epileptic encephalopathy, CDKL5 deficiency disorder. Epilepsy Res. https://doi.org/10.1016/j.eplepsyres.2020.106521
24. Li Y, Klena NT, Gabriel GC et al (2015) Global genetic analysis in mice unveils central role for cilia in congenital heart disease. Nature. https://doi.org/10.1038/nature14269
25. Liao Y, Wang J, Jaehnig EJ et al (2019) WebGestalt 2019: gene set analysis toolkit with revamped UIs and APIs. Nucleic Acids Res. https://doi.org/10.1093/nar/gkz401
26. Liao W, Lee K-Z, Chen J-C et al (2020) Deficiency of cyclin-dependent kinase-like 5 causes spontaneous seizures in neonatal mice. bioRxiv. https://doi.org/10.1101/2020.03.09.983981
27. Mirra V, Werner C, Santamaria F (2017) Primary ciliary dyskinesia: an update on clinical aspects, genetics, diagnosis, and future treatment strategies. Front Pediatr. https://doi.org/10.3389/fped.2017.00135
28. Mukherjee I, Roy S, Chakrabarti S (2019) Identification of important effector proteins in the FOXJ1 transcriptional network associated with ciliogenesis and ciliary function. Front Genet. https://doi.org/10.3389/fgene.2019.00023
29. Muthusamy N, Vijayakumar A, Cheng G, Ghashghaei HT (2014) A Knock-in Foxj1CreERT2: GFP mouse for recombination in epithelial cells with motile cilia. Genesis. https://doi.org/10.1002/dvg.22753
30. Negraes PD, Trujillo CA, Yu NK et al (2021) Altered network and rescue of human neurons derived from individuals with early-onset genetic epilepsy. Mol Psychiatry. https://doi.org/10.1038/s41380-021-01104-2
31. Noebels J (2015) Pathway-driven discovery of epilepsy genes. Nat Neurosci. https://doi.org/10.1038/nn.3933
32. Nuche-Berenguer B, Ramos-Álvarez I, Jensen RT (2016) The p21-activated kinase, PAK2, is important in the activation of numerous pancreatic acinar cell signaling cascades and in the onset of early pancreatitis events. Biochim Biophys Acta. https://doi.org/10.1016/j.bbadis.2016.02.008
33. Olson HE, Demarest ST, Pestana-Knight EM et al (2019) Cyclin-dependent kinase-like 5 deficiency disorder: clinical review. Pediatr Neurol. https://doi.org/10.1016/j.pediatrneurol.2019.02.015
34. Paz JT, Huguenard JR (2015) Microcircuits and their interactions in epilepsy: is the focus out of focus? Nat Neurosci. https://doi.org/10.1038/nn.3950
35. Pazour GJ, Agrin N, Leszyk J, Witman GB (2005) Proteomic analysis of a eukaryotic cilium. J Cell Biol. https://doi.org/10.1083/jcb.200504008
36. Rawlins EL, Ostrowski LE, Randell SH, Hogan BLM (2007) Lung development and repair: contribution of the ciliated lineage. Proc Natl Acad Sci USA. https://doi.org/10.1073/pnas.0610770104
37. Sattar S, Gleeson JG (2011) The ciliopathies in neuronal development: a clinical approach to investigation of Joubert syndrome and Joubert syndrome-related disorders. Dev Med Child Neurol. https://doi.org/10.1111/j.1469-8749.2011.04021.x
38. Schneider CA, Rasband WS, Eliceiri KW (2012) NIH image to imageJ: 25 years of image analysis HHS public access. Nat Methods. https://doi.org/10.1038/nmeth.2089
39. Shapiro AJ, Zariwala MA, Ferkol T et al (2016) Diagnosis, monitoring, and treatment of primary ciliary dyskinesia: PCD foundation consensus recommendations based on state of the art review. Pediatr Pulmonol. https://doi.org/10.1002/ppul.23304
40. Smith CL, Eppig JT (2012) The mammalian phenotype ontology as a unifying standard for experimental and high-throughput phenotyping data. Mamm Genome. https://doi.org/10.1007/s00335-012-9421-3
41. Smith CEL, Lake AVR, Johnson CA (2020) Primary cilia, ciliogenesis and the actin cytoskeleton: a little less resorption, a little more actin please. Front Cell Dev Biol. https://doi.org/10.3389/fcell.2020.622822
42. Staley K (2015) Molecular mechanisms of epilepsy. Nat Neurosci. https://doi.org/10.1038/nn.3947

43. Tam L-W, Ranum PT, Lefebvre PA (2013) CDKL5 regulates flagellar length and localizes to the base of the flagella in *Chlamydomonas*. Mol Biol Cell. https://doi.org/10.1091/mbc.e12-10-0718
44. Tang S, Wang I-TJ, Yue C et al (2017) Loss of CDKL5 in glutamatergic neurons disrupts hippocampal microcircuitry and leads to memory impairment in mice. J Neurosci. https://doi.org/10.1523/JNEUROSCI.0539-17.2017
45. Terzic B, Cui Y, Edmondson AC et al (2021) X-linked cellular mosaicism underlies age-dependent occurrence of seizure-like events in mouse models of CDKL5 deficiency disorder. Neurobiol Dis. https://doi.org/10.1016/j.nbd.2020.105176
46. Terzic B, Felicia Davatolhagh M, Ho Y et al (2021) Temporal manipulation of Cdkl5 reveals essential postdevelopmental functions and reversible CDKL5 deficiency disorder-related deficits. J Clin Investig. https://doi.org/10.1172/JCI143655
47. Tsukita S, Kunimoto K, Yamazaki Y et al (2012) Coordinated ciliary beating requires Odf2-mediated polarization of basal bodies via basal feet. Cell. https://doi.org/10.1016/j.cell.2011.10.052
48. Voss LJ, Sleigh JW, Barnard JPM, Kirsch HE (2008) The howling cortex: seizures and general anesthetic drugs. Anesth Analg. https://doi.org/10.1213/ane.0b013e3181852595
49. Wang ITJ, Allen M, Goffin D et al (2012) Loss of CDKL5 disrupts kinome profile and event-related potentials leading to autistic-like phenotypes in mice. Proc Natl Acad Sci USA. https://doi.org/10.1073/pnas.1216988110
50. Werner ME, Hwang P, Huisman F et al (2011) Actin and microtubules drive differential aspects of planar cell polarity in multiciliated cells. J Cell Biol. https://doi.org/10.1083/jcb.201106110
51. Yang J, Gao J, Adamian M et al (2005) The ciliary rootlet maintains long-term stability of sensory cilia. Mol Cell Biol. https://doi.org/10.1128/mcb.25.10.4129-4137.2005
52. Yoder SM, Dineen SL, Wang Z, Thurmond DC (2014) YES, a src family kinase, is a proximal glucose-specific activator of cell division cycle control protein 42 (Cdc42) in pancreatic islet β cells. J Biol Chem. https://doi.org/10.1074/jbc.M114.559328
53. Zuleta-Alarcon A, Castellon-Larios K, Moran K et al (2014) Anesthesia-related perioperative seizures: pathophysiology, predisposing factors and practical recommendations. Austin J Anesth Analg 2:1026